



## **1. Introduction**

With the development of high-speed and heavy-load railway, much higher requirements are put forward for the comprehensive properties of steel rails [1]. Since fracture accidents of steel rail threaten the safety of railway transportations directly, more and more attention is paid to the quality of rail steel. The fatigue fracture is the main failure form of steel rail. Despite substantial advantages in design, materials and non-destructive inspection, fatigue propagation in and failure of railway components remains an important issue for safety engineering which is also emphasized by a number of accidents over the last decades [2,3]. At the background of an increased volume of traffic, higher traffic speeds and higher axle loads, reliable damage tolerance design and effective maintenance methods have to be established. Therefore, failure analysis of the steel rail is very critical.

In addition to the fatigue load, rails are also subjected to other high mechanical loads and harsh environmental conditions. The main loading components are rolling contact pressure, shear and bending forces from the vehicle weight, thermal stresses due to restrained elongation of continuously welded rails and residual stresses from manufacturing (roller straightening) and welding in the field (Fig. 1) [2]. Welding is indispensable in the railway rail. Today, the most common rail

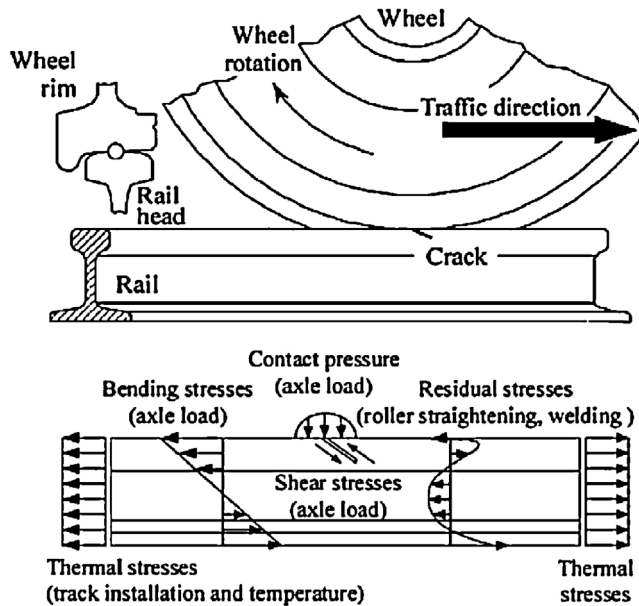


Fig. 1. Loading components acting at a continuously welded rail during vehicle passing [2].

welding processes are flash-butt welding, aluminothermic welding, gas pressure welding and enclosed arc welding. Among them aluminothermic welding of rails is used widely within the railway industry for in-track welding during re-rail and defect replacement. The process provides flexibility and low capital cost, but suffers from variable quality in finished welds, due to the inherent limitations of the processes used, and their operator dependency [4]. Therefore, it is harder to control the quality of welded points. Statistics show that during 18-month period aluminothermic weld failures comprise approximately 75% of all broken rail reports for the Newman mainline [4]. In response to failures in aluminothermic welds, and in recognition that such welds represent one of the main risks for a catastrophic derailment, it is necessary to develop an improved rail welding process which meets the performance demands of higher axle loads.

In the present paper, a fractured railway rail which was used for cargo trains was analyzed to find out its failure cause. In the end, a conclusion was reached after performing macroscopic inspections, chemical analysis, SEM observations, and metallographic examinations.

## 2. Background

Firstly, it is necessary to collect as much as possible the information on the previous history of the fractured railway rail. The fractured railway rail was provided by the railway administration staff. According to the introductions, the railway rail came into service in May 2005. The railway rails were butt-welded together by the aluminothermic welding process, and the postweld heat treatment was not conducted. The railway rail was found to be fractured in December 2011 when it was in winter. During 2005–2011, this route was serviced for heavy cargo trains. The type of the rail steel was GB P60U75V as introduced by the railway administration staff.

## 3. Results

### 3.1. Macroscopic inspections

The macroscopic fracture morphology of the fractured railway rail was shown in Fig. 2. The dimensions of the railway rail which were provided by the client were shown in Fig. 2(a). It was found that the fracture surface was basically clean and fresh, which demonstrated that the corrosion of the fracture surface was not heavy. The top in Fig. 2(a) was the railhead contacted with wheel rim, the bottom was the rail bottom contacted with the ballast, the middle part between railhead and rail bottom was the rail web. We could also found that the fracture surface at the rail bottom was close to the weld bead and relatively flat (Fig. 2(b)), and that the fracture surface was approximately perpendicular to the longitudinal direction of the railway rail. The fracture surface at the rail web was approximately arched when observed from the profile (Fig. 2(b)). The fracture surface at the railhead was inclined at about 60° to the longitudinal direction of the railway rail. The fracture surface at the railhead was very rough; therefore, it was deduced that this part might be caused by the final instant fracture instead of the fracture origin. There was a darkly fan-shaped area at the left bottom of Fig. 2(c). A small bright spot was observed next to the darkly fan-shaped area (Fig. 2(c)). As introduced by the railway administration staff, the bright spot was not separated yet when the railway rail failed.

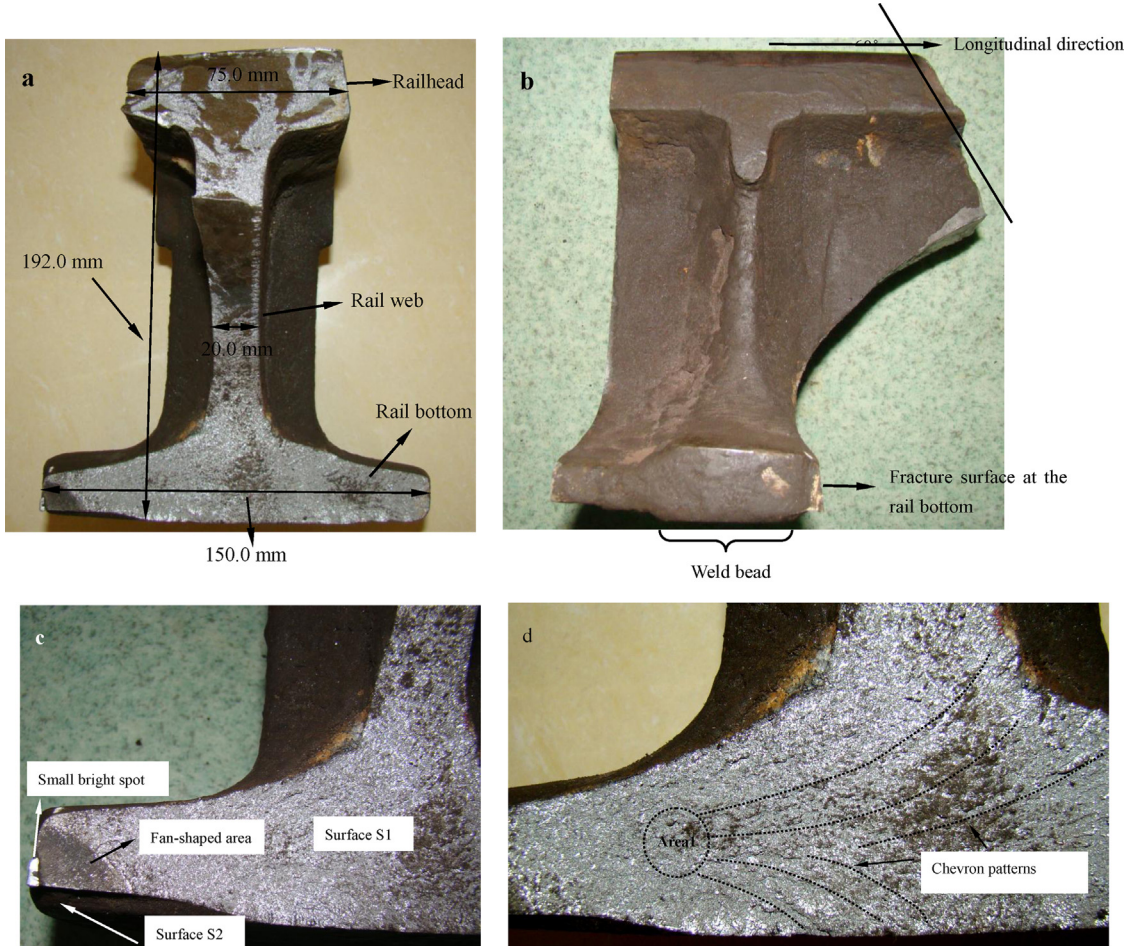


**Fig. 2.** The macroscopic morphologies of the failed railway rail. (a) The front view, (b) the lateral view, (c) the macroscopic morphology of the rail bottom, and (d) the chevron patterns and crack origin at the fracture surface of rail bottom.

Since the railway rail was subjected to cyclic loading and served about 6 years, it is rational to consider that this railway rail might be failed due to fatigue, even in giga cycle fatigue regime [5–7]. The arc boundary of fan-shaped area looks like a beach mark when observed macroscopically, as seen in Fig. 2(c). Then it can be deduced that the crack origin might be at the corner of darkly fan-shaped area (viz., the small bright spot as shown in Fig. 2(c)). However, taking into account that the small bright spot was next to darkly fan-shaped area, it is obviously to deduce that the small bright spot would not be the crack origin. The beach marks which were the classical features of metal fatigue were not observed from the macroscopic observations (the arc boundary of fan-shaped area is actually not a beach mark, we will discuss that hereinafter). However, the chevron patterns can be clearly observed at the fracture surface of rail bottom (Fig. 2(d)). Therefore, we can deduce that the crack origin should be at the tip of chevron patterns (area 1), and the crack growth direction is along the diverging direction of river patterns, as shown in Fig. 2(d). It can be deduced from the flat fractography and chevron patterns that the macro fracture feature is brittle fracture.

### 3.2. Chemical analysis

The sample used for chemical analysis which was sampled from railhead was analyzed by ZSX Primus II X-ray fluorescence spectrometer. The results were shown in Table 1. It was demonstrated that the chemical compositions of the

**Table 1**  
The chemical compositions of failed railway rail (mass%).

Steels	C	Mn	Si	S	P	V
The rail steel	0.74	0.96	0.68	0.0035	0.016	0.062
GB P60U75V	0.71–0.80	0.70–1.05	0.50–0.80	≤0.030	≤0.030	0.040–0.12

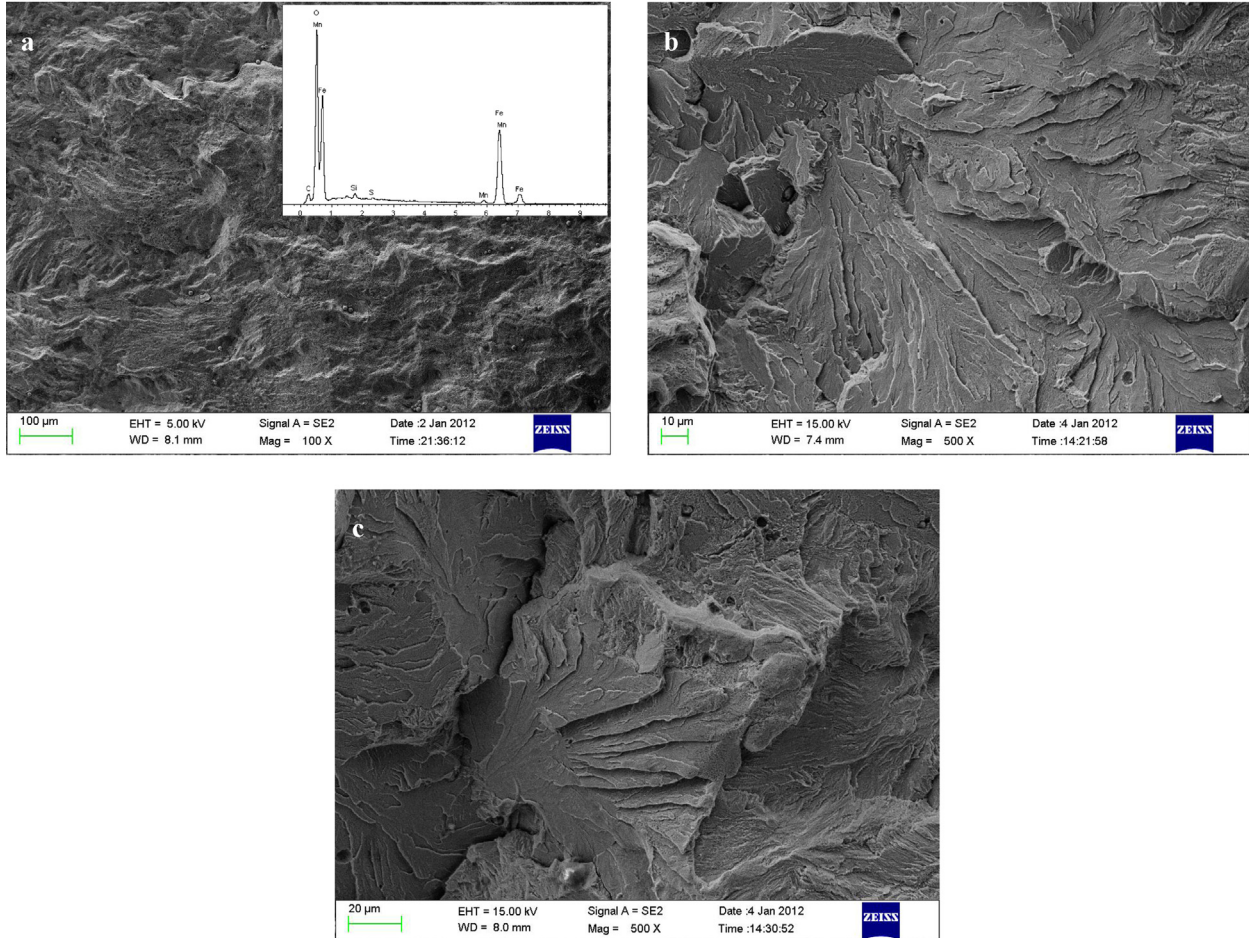


Fig. 3. The microscopic morphologies of the fracture surface. (a) Inside fan-shaped area, (b) area 1, and (c) the area of chevron patterns.

rail steel were in accordance with the standard of P60U75V [8]. Therefore, the compositions of the rail steel were normal.

### 3.3. SEM observations

The fracture surface at the rail bottom, viz. surface S1 (as shown in Fig. 2(c)), was cut from the failed railway rail, and then cleaned by alcohol and dichloroethane. After that, surface S1 was observed by ZEISS-SUPRA 55 field emission scanning electron microscope (FESEM) in detail. The morphology inside the darkly fan-shaped area is shown in Fig. 3(a) which shows a relatively flat surface. The qualitative chemical compositions of this area are analyzed by EDX, also shown in Fig. 3(a). Higher oxygen contents were detected, which demonstrates that this area was oxidized heavily. The typical morphology in area 1 is shown in Fig. 3(b) which shows the typical feature of cleavage fracture. The fan-shaped patterns, cleavage step and river patterns which are the typical feature of cleavage fracture are observed in this figure. Fatigue striations which were the typical microscopic features of metal fatigue were not observed in the fracture surface. The micro fractography of the chevron patterns area is shown in Fig. 3(c) which is similar to Fig. 3(b). The fracture surface outside the darkly fan-shaped area is clean and fresh, almost no oxygen is detected. Combined with the experimental results outside and inside the darkly fan-shaped area, it can be deduced that the darkly fan-shaped area might be an incomplete fusion area during welding.

### 3.4. Metallurgical observations

Firstly, surface S2 (as shown in Fig. 2(c)) was polished to observe the distribution of inclusions. It was shown in Fig. 4 that some bigger slag inclusions with sharp angular shape were observed at surface S2 close to the fracture surface at the rail bottom. The size of these slag inclusions was about at least 126 µm defined by Murakami's effective projective area model [9]. EDX demonstrated that the composition of these slag inclusions was alumina. After etched by 3% nital the metallurgical structure of surface S2 close to the fracture surface was observed by optically metallurgical microscope (OMM). Continuous

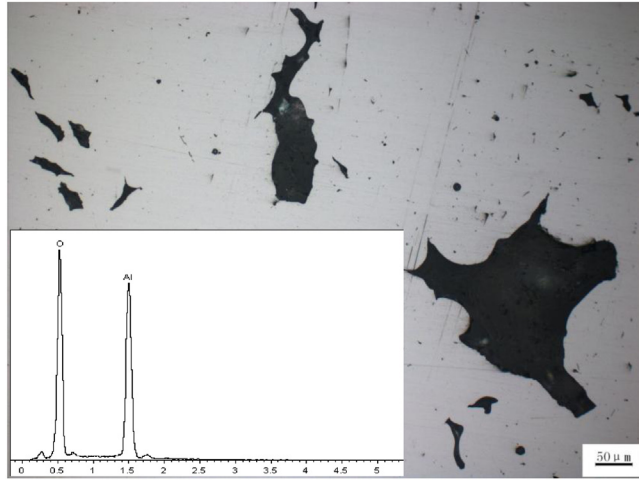


Fig. 4. The morphologies of the slag inclusions and EDX results.

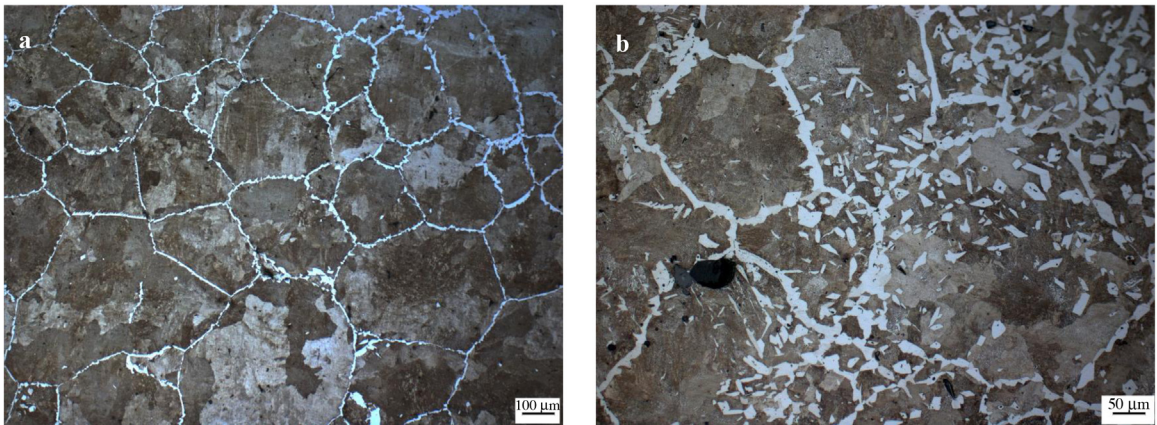


Fig. 5. (a) The metallurgical structures of surface S2 close to the fracture surface and (b) the metallurgical structures in area 1.

ferrite networks and pearlite colonies were observed, as shown in Fig. 5(a). It was also demonstrated from Fig. 5(a) that the size of pearlite colony, viz. the area surrounded by continuous ferrite networks, was rather heterogeneous. The biggest size of the pearlite colony was about 726  $\mu\text{m}$  in diameter, the smallest size 68  $\mu\text{m}$ . After making an obvious mark at the crack origin site (area 1) on surface S1, surface S1 was polished and etched by 3% nital in order to observe the metallurgical structures. The metallurgical structures in area 1 were pearlite, continuous ferrite networks and a mass of ferrite fragments distributed inside the pearlite colonies, as shown in Fig. 5(b). Considering the weaker strength of ferrite distributed like nets compared with pearlite; it can be deduced that the crack might be initiated from the ferrite networks.

#### 4. Discussion and analysis

As introduced in Section 1, the railway rail was mainly subjected to cyclic loading. In this case study, the macroscopic beach marks and microscopic fatigue striations were not observed at the fracture surface. In addition, the typical chevron patterns were observed. And the feature of cleavage fracture was observed at the tip of chevron patterns. Given all of that, we can draw a conclusion that the railway rail is mainly caused by overload even though it is subjected to cyclic loading. Considering the abnormal metallurgical structures (ferrite networks distributed along the grain boundaries) at the crack origin, the crack is supposed to be initiated from the weaker ferrite networks which are caused by welding. Therefore, it is much needed to eliminate the ferrite networks by improving the welding technology.

In this case study, this railway rail was mainly subject to alternate bending stress due to vehicle weight, as shown in Fig. 1. It is shown from Fig. 1 that the rail head was subject to compressive stress and the rail bottom was subject to tensile stress.

Therefore, the rail bottom was subtle to fail from the point of view of mechanics. The rail bottom can be approximately considered to subject fatigue load in the longitudinal direction of railway with  $R = 0$  ( $R$  was stress ratio), and the applied stress at the lower bottom of rail was approximately the maximum. In view of the heavily incomplete fusion area (darkly fan-shaped area in Fig. 2(a)) at the bottom corner of rail bottom, the crack was supposed to be initiated from this incomplete fusion area. Nevertheless, in fact it is not the case. The residual stress must be considered. In addition to the residual tensile thermal stress due to track installation and temperature (as shown in Fig. 1), the welding residual stress was also of great importance. The welding residual stress was usually detrimental; therefore, many rail failures were initiated from the weld [4]. The residual stress and applied stress due to the train's gravity can be superimposed together. The superimposed stress will induce the failure of the rail under certain conditions.



## **1. Introduction**

High strength low alloy (HSLA) steel with a nominal composition of 0.15C–1.25Cr–1Mo–0.25V is being extensively used in space programme. Owing to its ease of fabrication and welding, a tank was fabricated out of this alloy. The tank is used to contain strontium per chlorate which on combustion develop secondary thrust, effectively used during attitude control of satellite launch vehicle. During one of the routine qualification tests, a tank had failed at an internal pressure of 109 bar, against a designed proof pressure of 120 bar.

Failure was initiated from long seam weld of a cylindrical shell and propagated into the parent material thereafter. Detailed metallurgical investigation has been carried out to understand the cause of failure. This paper brings out the detail of investigation carried out.

## **2. Material**

The 700 mm diameter pressure vessels were fabricated using 6.2 mm thick cold rolled sheet of required dimensions. The tank had three cylindrical shells of which each shell was fabricated by roll bending the cold rolled sheets and through long seam welding. These cylindrical shells were welded circumferentially welded to configure the main cylindrical tank. The

shell is hardened through heat treatment at 975 °C, 20 min/oil quenched and tempered at 640 °C, 40 min/air cooled. Two rings, one at both ends (dome side as well as nozzle side) were welded to cylindrical portion of shell to provide the necessary rigidity as per design requirement. This resulted in configuration of 700 mm dia. tank of 4.6 m length and it had a mass of approximately 590 kg. The tank so configured had maximum effective operative pressure (MEOP), proof pressure, minimum burst pressure (MBP) are 80, 120 and 160 bar respectively. Total 6 tanks were fabricated and tested for proof pressure testing (PPT). Out of six, one had pre-mature failure while remaining five were successfully withstood the test and inducted into the system.

### 3. Observations

Failed tank was observed at the site of failure. Out of three shells of the tank, failure occurred in one shell, while remaining two were intact (Fig. 1). First hand observation indicated that failure initiated at long seam of the shell, near shell-ring



**Fig. 1.** Photographs showing failed tank, (a and b) failed shell and (c) failed shell with other two intact.

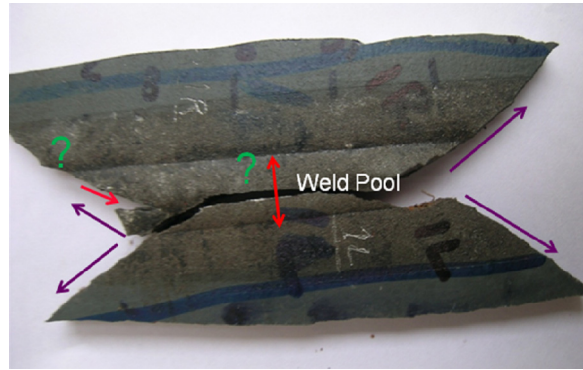


Fig. 2. Failure initiation at weld pool and further propagation into the parent on either side making an angle of 45° to weld line.

cir-seam joint. The fracture, subsequent to little travel along weld pool, propagated into the parent on either side making an angle of 45° approximately to weld line (Fig. 2). At the ring side, the crack had deviated its path and propagated in a circumferential direction running parallel to and very close to the circumferential weld for a length of approximately 160 mm. A schematic sketch of the fracture travel path of tank is shown in Fig. 3. The remaining material in failed shell has been grouped as left side (A), right side (B) and side (C). Thickness all along the fracture path and at the interval of approximately 20 mm apart on all the three material segments at locations 1–33 on left side 'A', 1–32 on right side 'B' and

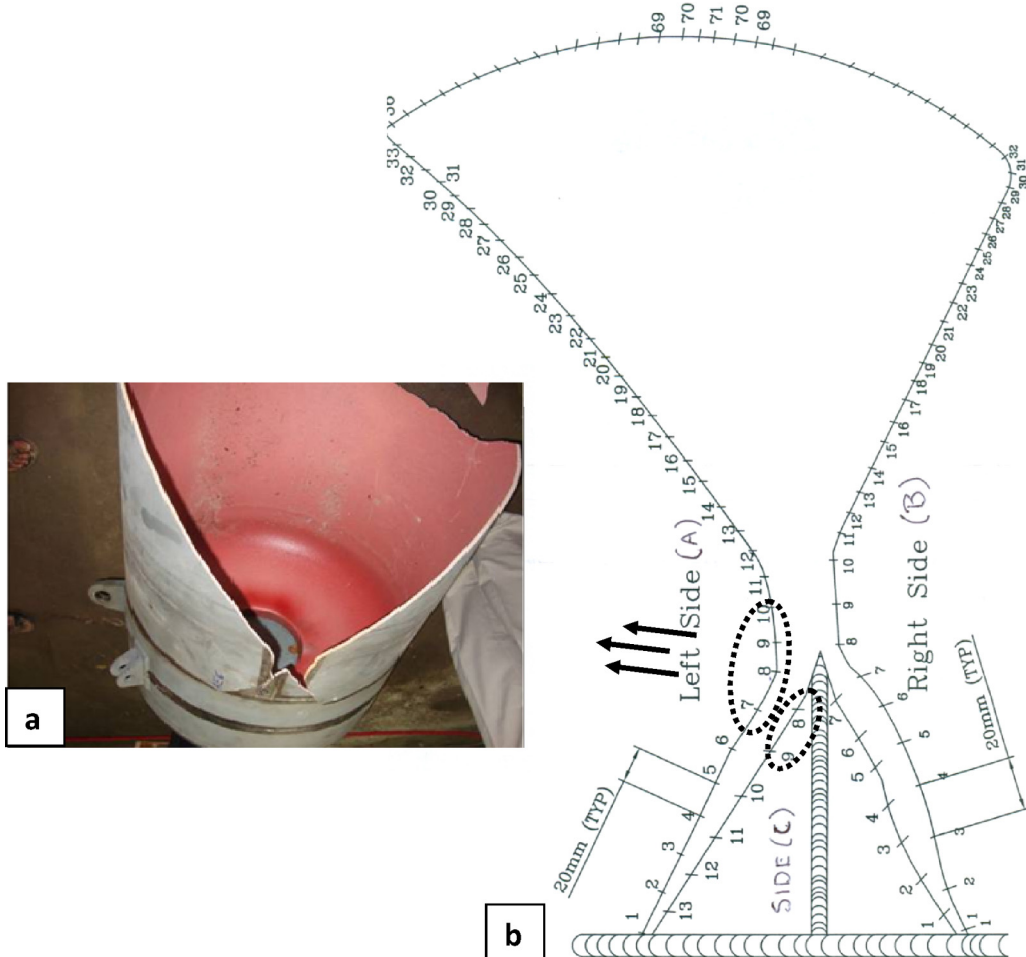


Fig. 3. (a) Photograph of failed shell and (b) schematic sketch of fracture edge all along and the location identification for thickness measurement.

**Table 1**

Thickness measured on left side (A) and right side (B) at 10 mm apart.

Locations	Left side (A)	Right side (B)
	Thickness in mm	
1	5.97	6.07
2	6.04	6.28
3	6.00	6.25
4	5.95	6.14
5	5.96	6.19
6	5.93	6.15
7	<b>5.72</b>	5.90
8	<b>5.74</b>	5.95
9	<b>5.79</b>	6.10
10	6.13	5.90
11	5.90	6.05
12	5.99	6.18
13	5.99	6.05
14	5.96	6.12
15	5.93	6.18

Bold value indicate thinnest region.

**Table 2**

Thickness measured at location side 'C' at 10 mm apart.

Location	Side 'C'	
	Thickness in mm	
1	6.15	
2	6.20	
3	6.20	
4	6.16	
5	6.21	
6	6.01	
7	6.08	
8	<b>5.92</b>	
9	<b>5.90</b>	
10	5.98	
11	6.05	
12	6.09	
13	6.11	

Bold value indicate thinnest region.

1–13 on side 'C' was measured using ultrasonic testing gauge and reported. Thickness at locations 1–15 on left side 'A' and 1–13 on side 'C' were of our concern, as they were around the failure origin and tabulated in [Tables 1 and 2](#) respectively.

The typical values of thickness measurement (at locations of our interest) on material segment 'left side (A)' and 'right side (B)' is reported in [Table 1](#), while that of material segment 'C' is furnished in [Table 2](#). The thickness measured at locations 7, 8, 9 on left side 'A' and 8, 9 on side 'C' had minimum thickness in the range of 5.72–5.90 mm, whereas other locations had thickness in the range of 5.90–6.20 mm. This indicated thinning of material at above locations. It is interesting that these locations fall very near to/coincided with the long seam weld of shell, where initially crack initiation was postulated. At locations 7, 8, 9 of material segment 'A', thickness measurement was further carried out at locations starting from fracture edge to interior of material at the interval of 2–3 (approx.) mm apart. The measured thickness is reported in [Table 3](#). Measurement further confirmed predominate thinning at these locations.

**Table 3**

Thickness measured from fracture edges to interior of material at 2–3 mm apart.

Location '7'	Location '8'	Location '9'
5.72	5.74	5.79
5.72	5.78	5.81
5.80	5.80	5.81
5.80	5.84	5.86
5.81	5.89	5.90
5.84	5.94	5.92
5.88	5.96	5.95



Fig. 4. Specimens taken out from locations 1L, 1R, 2, 3 and 4.

Fracture surface was studied using scanning electron microscope. Specimens were selected for fracture studies from location 1 (L and R) at region of long-seam weld, location 2 (at region of cir-seam weld; shell-ring weld) parting, location 3 and 4 (from region away from fracture initiation site), as shown in Fig. 4.

The fracture surface at location '1L' and '1R' under optical microscope with stereomicroscopic facility revealed the semi elliptical featureless region (Fig. 5). The region was about  $7\text{ mm} \times 2\text{ mm}$  towards the inner surface of tank and hence confirmed to be at weld root. Remaining region of fracture surface had features of directionality as if crack initiated from this featureless region and propagated radially through thickness of the steel (Fig. 5). The featureless region was viewed under scanning electron microscope and confirmed to be lack of fusion (LF) during welding operation (Fig. 6). At many locations

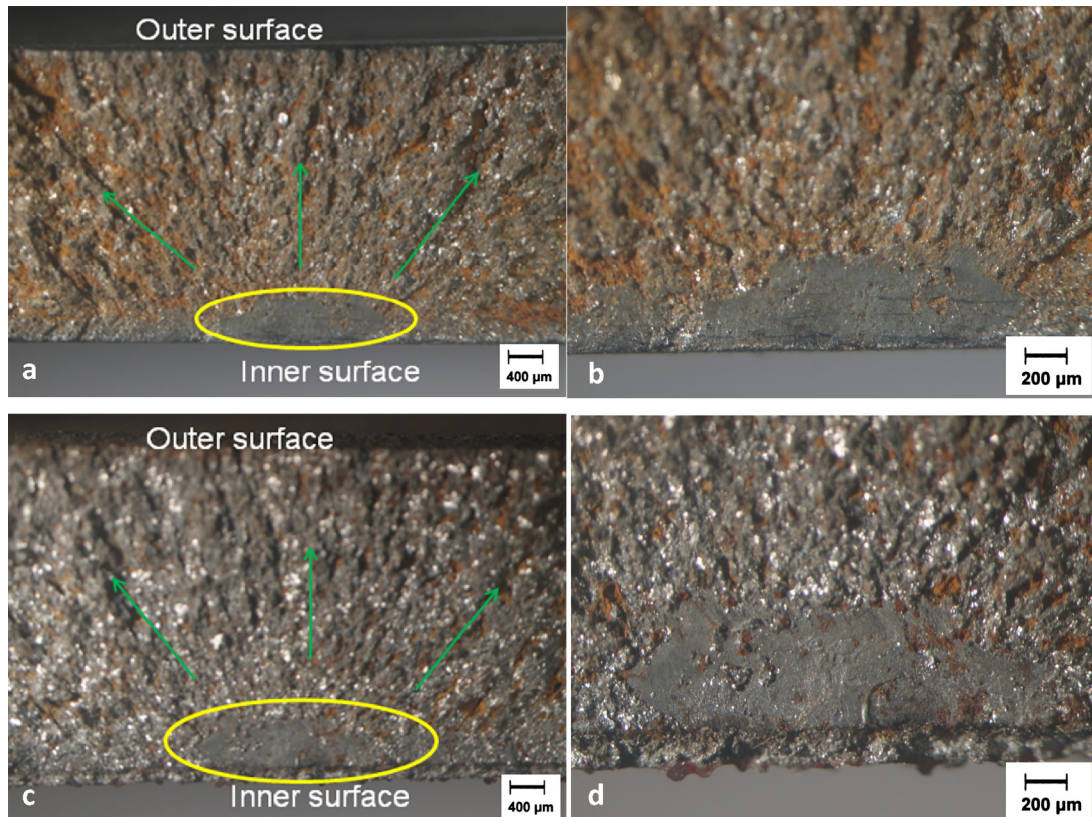
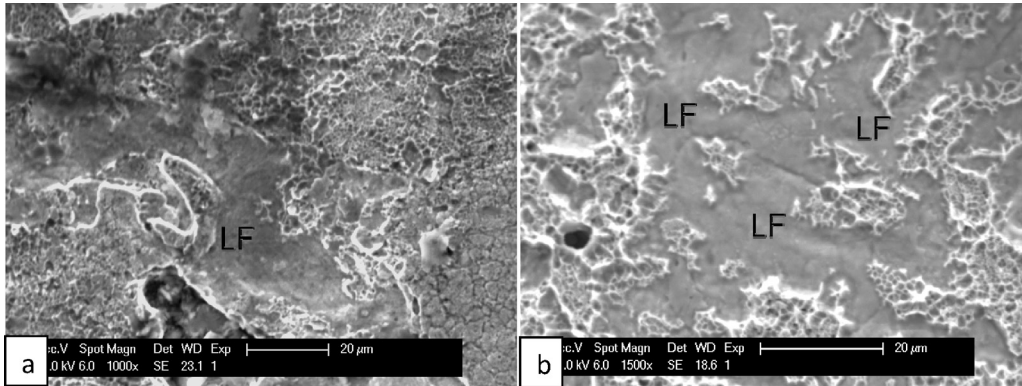
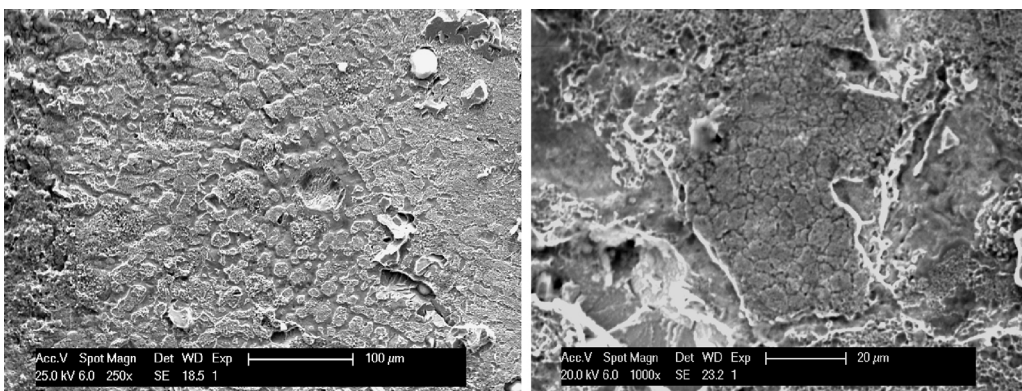


Fig. 5. Optical photo macrographs showing featureless semi-elliptical region on fracture surface (a and b) on specimen 1R and (c and d) on specimen 1L.



**Fig. 6.** SEM fractographs showing lack of fusion within fracture initiation region.



**Fig. 7.** SEM fractographs showing dendrites resulted from solidification of insufficient metal liquid.

denritic pattern, resulted from solidification of insufficient liquid was also seen (Fig. 7). The fracture surface beyond this region had ductile tearing and quasi cleavage facets (Fig. 8), typical of ductile overload mode of failure. The elongated micro voids became tear dimples formed in narrower band a head of well defined crack front (Fig. 9). There was shear lip at both the fracture edge, as confirmed by elongated dimples on slant fracture (at 45°) surface (Fig. 10). The cut piece was removed from the failed tank for microstructure study. Specimens were polished using conventional metallographic technique. The specimen duly etched with 3% Nital revealed microstructure typical of hardened and tempered steel (Fig. 11).

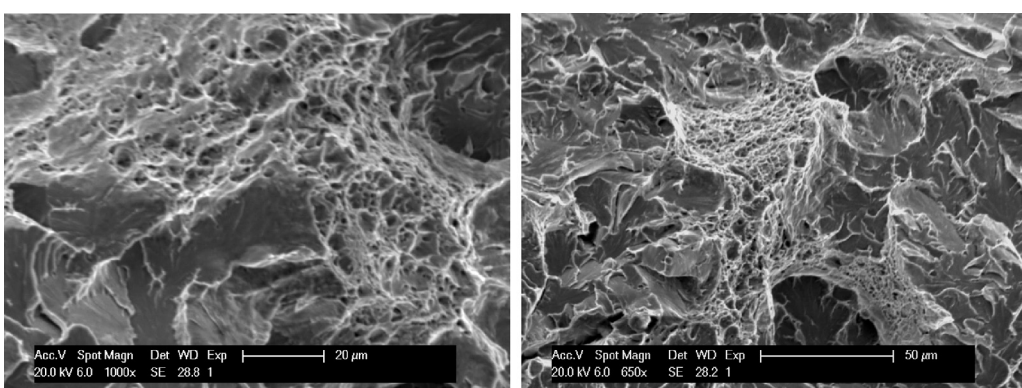


**Fig. 8.** SEM fractographs showing ductile tearing with quasi cleavage facets.

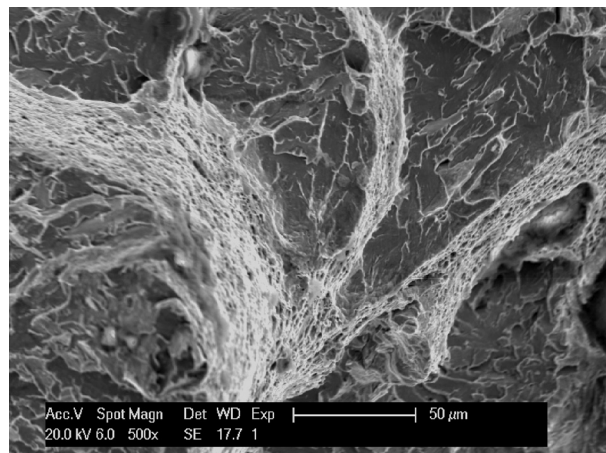


Fig. 9. SEM fractograph showing tearing dimples resulted from elongated micro voids ahead of crack front.

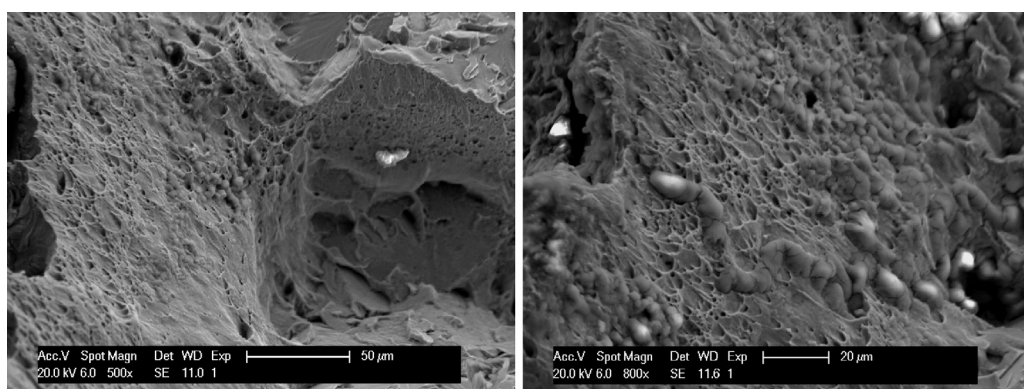


Fig. 10. SEM fractographs showing elongated dimples within shear lips on either side of fracture surface.

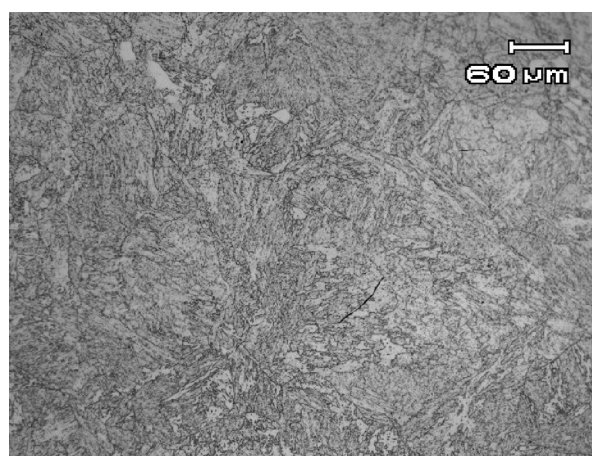


Fig. 11. Optical photomicrograph showing tempered martensite.

### 3.1. Mechanical property evaluation

Tensile specimens fabricated from shell portion of failed tank were tested for mechanical properties evaluation. The location of specimen taken, and the values obtained is furnished in [Table 4](#). Specimens were taken from the fractured shell, in such a way that the specimens with identification 'TP' fall in direction perpendicular to sheet rolling direction, or otherwise

**Table 4**  
Mechanical properties of specimens taken from failed tank.

Specimens	UTS (MPa)	0.2% PS (MPa)	%El (50 mm GL)
TP: parent $\perp^r$ to rolling direction	939–962	838–846	15.7–16.6
TW (CS): with cirseam weld at centre	887–962	784–863	11.6–13.4

perpendicular to cirseam weld (shell to shell) and TW(CS) is similar to specimen 'TP' except the cirseam weld pool was within gage length of the specimens.

#### 4. Discussions

The tensile properties and the microstructure of the material confirmed that material was in hardened and tempered condition. Chemical constituents of material used were well within the specification. Considering all above observations together, the only possibility is that the weld discontinuity (flat, featureless facets at long seam weld root) of shell have acted as the origin of fracture. The presence of features typical of fracture directionality and that too pointing towards this featureless region further confirmed this to be the origin of failure. Weld discontinuities may be linked with many sources in welding, like improper geometry, wrong welding process and metallurgical discontinuity. The type of discontinuity seen in the present case and the features evidenced were confirmative of lack of fusion.

The immediate consequences of this is that the cross sectional area of the weld reduces below the designed value and therefore it becomes a point of weakness [1]. The thickness of the ligaments at the material segment 'A' and 'C' had severe thinning near the region of this lack of fusion. Similar type of premature failure of a high strength low alloy steel pressure chamber was studied by Sharma et al. [2]. Welding defect growing to a semi elliptical surface crack, resulting in localised thickness reduction and acting as stress raiser was attributed to be possible cause of failure.

549707

## 1 Background

The article reports a failure in high-strength low alloy (HSLA) steel pressure vessel, which was used to store strontium perchlorite used as fuel in satellite launches. The pressure vessel suffered a fracture during a routine qualification test. Six identical pressure vessels were manufactured, out of which only one failed.

The tank was manufactured from three pieces of 6,2 mm cold rolled sheet metal, which were bent to form cylinders 700 mm in diameter. The cylinders had one lengthwise seam connecting the ends of the steel sheet, and the cylinders were joined with circumferential welds. The cylindrical section of the vessel was hardened by holding it at 975°C for 20 minutes before oil quenching and tempered by holding it at 640°C for 40 minutes before air cooling. The ends of the pressure vessel consisted of reinforcement rings and end caps, both joined to the cylindrical section with circumferential welds.

The tank failed at the pressure of 109 bar, while it had maximum effective operation pressure (MEOP) of 80 bar, proof pressure of 120 bar, and minimum burst pressure of 160 bar. The failure was a fracture that started from a lengthwise weld seam in a cylindrical section close to one end of the tank. The crack propagated in four directions from the starting point in an X-shaped manner. Two of the cracks extended around the cylindrical section, splitting the tank into two parts, while two cracks propagated towards the end cap, but did not cross the weld seam into the reinforcement ring welded between the cylindrical section and the end cap.

## 2 Investigation methods

Wall thickness of the tank was measured in 10-20 mm intervals along the edges of the fracture with an ultrasonic gauge. The measurements revealed that the wall thickness was below the specification of 6,2 mm everywhere around the crack origin, being 5,72 mm at the lowest.

Fracture surface was studied with optical macrographs and a scanning electron microscope (SEM). Optical micrographs revealed that at region where the crack was suspected to have originated, there was a semi-elliptical featureless region adjacent to the inner surface of the tank.

The tank was welded from outside and the crack was centered over the longitudinal weld, which places the suspected origination point at the weld root.

SEM imagining of the suspected initiation region showed flat, featureless regions, which suggest incomplete fusion at the weld root. Furthermore, there were dendrites, which suggest that the weld pool was not formed properly.

SEM imagining of the fracture surface revealed partly ductile, partly brittle fracture surface, typical to an overloading situation. Elongated dimples suggest that shear stress was present as well. Microstructure samples were prepared by polishing and etching and investigated using light microscopy, revealing tempered martensitic microstructure.

Mechanical properties of the material were also investigated with tensile test, but the article provides no information if the properties are within specification. Chemical composition of the material is claimed to be within specification, but there is no information as to how it was tested.

### 3 Primary cause

The article concludes that the cause of the failure was overloading fracture caused by a welding defect. There was lack of fusion in the weld root, which caused stress concentration. As the tank was pressurized over the maximum effective operating pressure during testing, the stress exceeded what the material could withstand, and the tank burst. The partly ductile, partly cleavage fracture surface, elongated dimples near shear lips, and thinning of the tank walls near the fracture all support this theory.

### 4 Alternate mechanisms

Creep effects start to appear if the material is exposed to stress in temperature exceeding 0,3\*melting point, which was not the case here, ruling creep out.

The tank was not subjected to a high number of pressurization cycles, as the failure occurred during an over pressurization test in qualification testing, not during operation or a fatigue test. The fracture surface also did not showcase any beachmarks, ruling out fatigue.

The tank was designed for storing strontium perchlorate, which is a strong oxidizer and could possibly cause corrosive stress. However, as the tank never entered operation, it was likely not exposed to strontium perchlorite or corrosive operation environment, ruling out environmentally assisted failure.

### 5 Preventing further similar failures

Careful consideration of welding parameters and the welding process could reduce the risk of welding defects. The welds could be inspected with NDT such as eddy current testing or ultrasonic testing before qualification testing, to allow repairing defects before the tank is subjected to conditions that could cause an overloading failure if defects are present. However, the issue was caught before the tank entered operation, in which sense a failure was already prevented by the testing procedure.



## **1. Introduction**

Axles are connected within vehicles to perform two important functions: (i) they transmit torque from variance to wheel through planetary gear arrangement, and (ii) they maintain the position of the wheels comparative to each other and to the body of the vehicle. In most non-commercial vehicles, the circular motion of the drive wheels is maintained by means of axle shafts, which are integral component of the rear axle [1]. The shafts are installed in the tire's wheel well near the differentials and stretch across the bottom of the vehicle. Often during operation, the axle shafts are subjected to heavy torque due to loads or sudden acceleration and therefore, they are manufactured from different grades of hardened steels. There were four numbers of such axle shafts in service at the fork lift, out of which two failed. The fork lift is used to lift wire rod coils from the coil yard. An axle shaft of fork lift failed at operation within 296 h of service. No damage was reported in the other components of the assembly. Sudden jerk was observed before failure, which might be due to the effect of overloading. The fractured shaft with a diameter of about 7 cm was manufactured by the forging of 42CrMo4 grade of steel given an induction

hardening treatment to produce a case of 3–4 mm in depth as per specification. A section of fractured rear axle shaft was removed from the location to determine the most feasible cause of failure.

## 2. Experimental procedure

The failed axle shafts were collected from the plant for investigations. The samples were cleaned with acetone to remove dirt for visual examination prior to metallographic sample preparation. Transverse and longitudinal specimens were made from the fractured end of the failed samples for conducting optical microscopic examination. These samples were individually mounted in conductive mounting and polished by conventional metallographic techniques for scratch free surface. The polished samples were etched in 3% Nital solution (3 mL HNO<sub>3</sub> in 97 mL ethyl alcohol), and both un-etched and etched samples were examined under an optical microscope. The micro-hardness of different location which was observed in the failed samples was determined in a pneumatically controlled automatic micro hardness tester (Leco-LM247<sub>AT</sub>). An applied load of 100 gf was used during testing, and several indentations were made to determine the hardness of the failed component. Field Emission Gun Scanning Electron Microscopy (FEG-SEM) of the samples was also carried out to identify exact phases present in the samples. The analyses were performed at 15 keV accelerating voltage and 5<sup>10<sup>-8</sup></sup> A probe current.

## 3. Results and discussions

### 3.1. Visual observation

**Fig. 1a** is a schematic illustration of the rear axle shaft showing the approximate location of the fracture near the wheel mounting flange. A photograph of the section received for analysis is shown in **Fig. 1b**. The axle shaft failed in shear mode at almost 45° to the longitudinal direction under torque [2,3]. It is observed that the fracture surface consists of two distinct regions: (i) a relatively smooth annular region at periphery marked as A where the fracture was initiated, and (ii) a rough core marked as B (shown in **Fig. 1c**).

### 3.2. Chemical analysis

The chemistry of the failed axle shaft matches with 42CrMo4 grade of steel. Chemical analyses of the failed sample are given in **Table 1**.

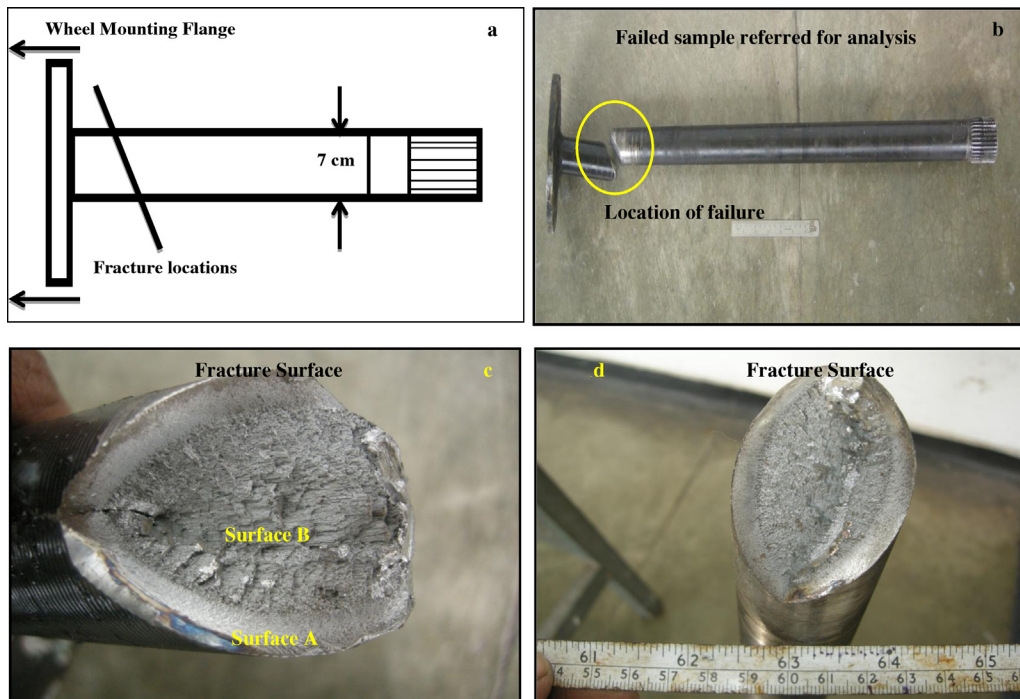


**Fig. 1.** (a) Schematic illustration of the rear axle shaft showing the approximate location of the fracture near the wheel mounting flange; (b) general view of the failed axle shaft referred for analysis; (c) closer view of the fracture surface of the failed component.

**Table 1**  
Particulars of failed samples.

Sample type	C	Mn	S	P	Si	Cr	Mo	Dia. (cm)
Failed shaft	0.415	0.785	0.03	0.01	0.255	1.045	0.172	7.0
Specification (42CrMo4)	0.38–0.45	0.60–0.90	0.035 max	0.025 max	0.40	0.9–1.2	0.15–0.3	

### 3.3. Fractography

Fractography of the outer surface (region A) revealed cleavage nature of the fracture surface suggesting brittle fracture ([Fig. 2a](#)), whereas the fractography of the inner core (region B) revealed dimple nature of the fracture surface suggesting ductile fracture ([Fig. 2b](#)).

### 3.4. Microstructural analysis

The failed sample was etched with 2% Nital solution. The macrostructure at the cross-section of the rod reveals case hardened layer as the component was subjected to induction hardening treatment ([Fig. 3a](#)). The hardening layer was non-uniform along the cross-section and in some location it was found more than the specification (>2–3 mm). The un-etched microstructure reveals numerous sulphide inclusions throughout the sample which indicates that the steel is not clean ([Fig. 3b](#)). The surface of the rod sample reveals in-homogeneous/banded microstructure in martensitic matrix ([Fig. 3c](#)), whereas the core reveals ferrite pearlite structure ([Figs. 3b](#)). Mixture of coarse and fine pearlite structure was observed in the core of the sample which was resulted due to improper heat treatment process.

### 3.5. Inclusion rating

Inclusion rating of the failed component was carried out as per ASTM E-45. Un-etched microstructure of shaft shows that thin and thick sulphide (Type A) inclusions are present with a severity of 2.5 and 0.5 respectively. Some inclusions of Type D (oxides) are observed with a severity of 0.5. Such a huge number of inclusions are not desirable as they can act as stress concentration sites and may lead to crack initiation (as shown in [Table 2](#)).

### 3.6. FEG-SEM analysis

Non-metallic inclusions were observed along the longitudinal axis of the component. Elemental analysis under SEM reveals that the inclusions were found to be rich in Sulphur (S) and Manganese (Mn) indicating them to be manganese sulphide inclusions (as shown in [Table 3](#)). The crack in this region has propagated by brittle mode and MnS inclusions could have enhanced the notch sensitivity of the shaft [4–6] ([Fig. 4](#)).

### 3.7. Hardness profile

Non-uniform distribution of hardness was observed in the rod sample across the section ([Fig. 5](#)). The average hardness of the surface hardened layer is measured to be 735 HV which is very high compared to the core and also for these applications. Such high hardness is not desirable since it imparts brittleness.

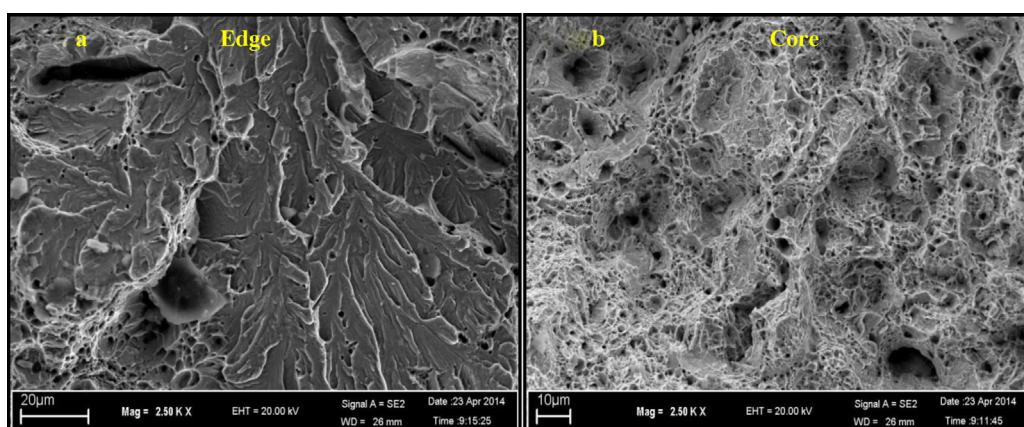


**Fig. 2.** (a) Fractography analysis of side A of the failed component; (b) fractography analysis of side B of the failed component.

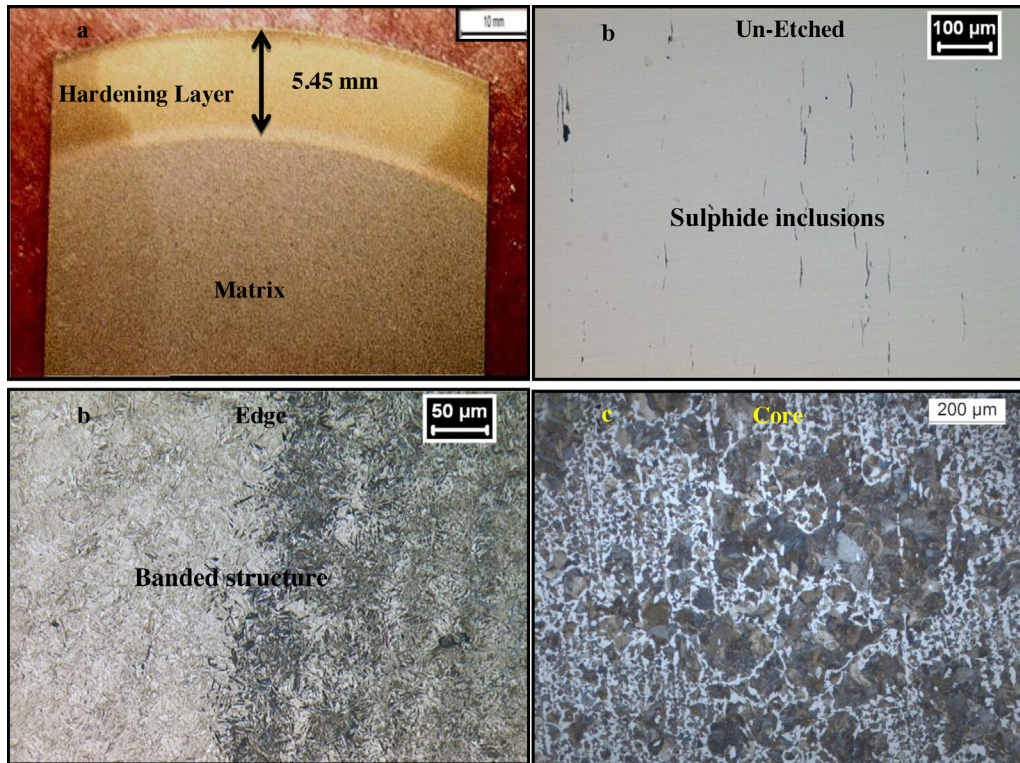


Fig. 3. (a) Macrostructure of the cross-section of the failed shaft; (b) un-etched structure of the failed shaft; (c) microstructure of the edge of the component; (d) microstructure of the edge of the component.

#### 4. Discussions

The fork lift is used to lift wire rod coils from the coil yard. No damage was reported in other components of the assembly. The fractured shaft with a diameter of about 7 cm was manufactured by forging of 42CrMo4 grade of steel given an induction hardening treatment to be producing a case of 3–4 mm in depth as per specification. A section of fractured rear axle shaft removed from the location was received to determine the most feasible cause of failure. The axle shaft failed on shear mode at 45° to the longitudinal direction under torque. It is observed that the fracture surface consists of two distinct regions: (i) a relatively smooth annular region at periphery marked as A where the fracture was initiated, and (ii) a rough core marked as B. Fractography of the outer surface (region A) revealed cleavage nature of the fracture surface suggesting brittle fracture, whereas the fractography of the inner core (region B) revealed dimple nature of the fracture surface suggesting ductile fracture. The macrostructure at the cross-section of the rod reveals case hardened layer as the component was subjected to induction hardening treatment. The hardening layer was non-uniform along the cross-section and in some location it was found more than the specification (>2–3 mm). The un-etched microstructure reveals numerous sulphide inclusions

**Table 2**  
Inclusion rating.

Sample	A (thin/heavy)	B (thin/heavy)	C (thin/heavy)	D (thin/heavy)
Axle shaft	2.5/0.5	0.0/0.0	0.0/0.0	0.5/0.0

**Table 3**  
EDS analysis (wt.%).

Spectrum	S	Mn	Total
1	37.83	62.17	100.00
2	38.62	61.38	100.00

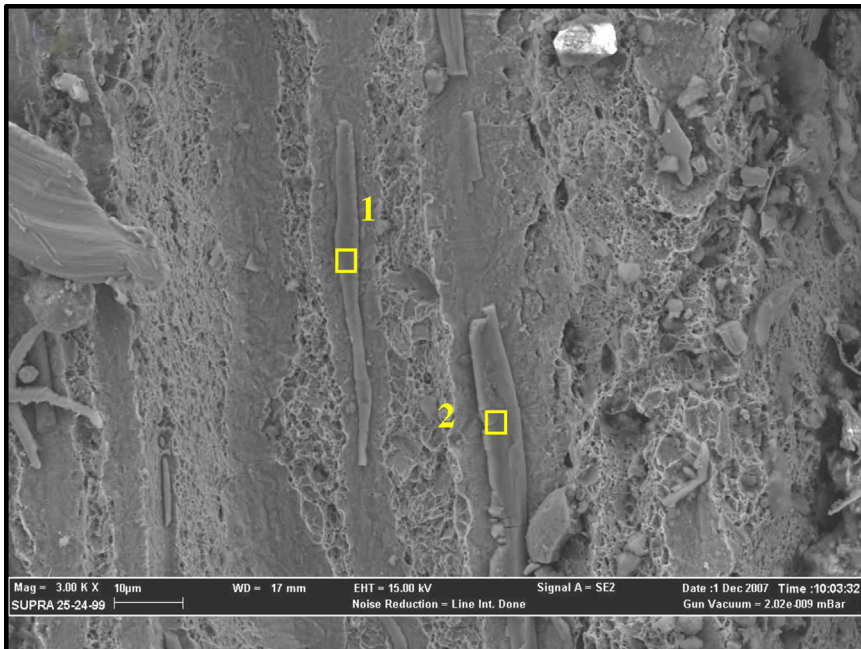


Fig. 4. The fracture surface shows multiple sulphide stringers oriented in the direction of crack propagation.

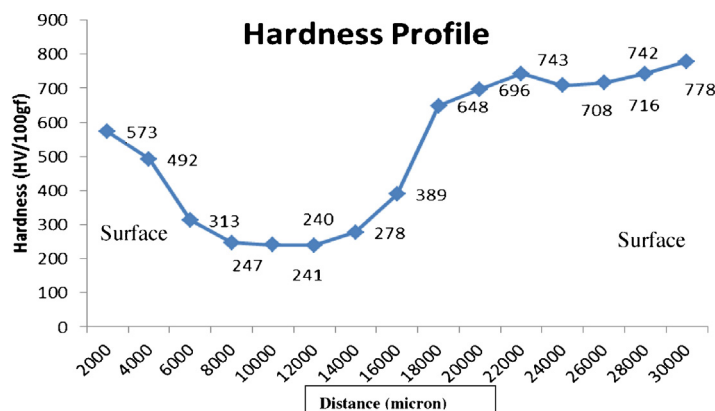


Fig.5.Thehardnessprofileofthetransversesectionoftheshaft.

throughout the sample which indicates that the steel is not clean. The surface of the rod sample reveals in-homogeneous/banded microstructure in martensitic matrix, whereas the core reveals ferrite/pearlite structure. Mixture of coarse and fine pearlite structure was observed in the core of the sample which resulted due to improper heat treatment process. The difference in fracture behaviour is caused by variation in microstructure of the case and core resulting from the improper hardening treatment. Due to improper heat treatment of the shaft which is resulting in case microstructure with poor ductility due to high hardness which results in the material more susceptible to brittle fracture. Non-metallic inclusions were observed along the longitudinal axis of the component. Elemental analysis under SEM reveal that the inclusions were found to be rich in Sulphur (S) and Manganese (Mn) indicating them to be manganese sulphide inclusions (as shown in Table 3). The crack in this region has propagated by brittle mode and MnS inclusions could have enhanced the notch sensitivity of the shaft.

887799

# Materials safety: article exercise

You are working as a materials expert in your organization and your responsibility is to guarantee safe and efficient use of materials in your facility. One day, a failure in similar facility is brought to your attention, and you need to investigate the possible implications this failure has for your facility. Your job is to interpret and analyze the given failure report and to write a report, which will allow others in your organization to understand the key developments and causes leading to the failure and the necessary actions for prevention of such failures.

Read the given article and analyze the failure. Describe, how the deformation and failure mechanisms presented during the course are reflected in the case and establish the chain of actions leading to the failure. The report should work as an introductory material to your team; it should not be very long but it should enable other team members to understand the key features of the failure without reading the failure report itself.

In addition to establishing the primary cause of the failure, show why alternate failure mechanisms can be ruled out. Some failure mechanisms have not been discussed in the course yet. Conduct the analysis using your present knowledge on the subject.

If the author of the failure analysis has, in your view, neglected to address some aspects of the failure, you may indicate this in your report and suggest tests or actions that should have been done to clarify the issue.

Prepare your response by editing this word document and export it as PDF. The file name identifies you and the article. Do not change the file name (other than the extension to pdf). E-mail the pdf to "materials.safety@iikka.fi".

You may use the question list below to guide you in your analysis:

- A. Description of investigation methods applied
  - What means of investigation were used in the failure analysis?
  - What computational methods were used?
  - What material or results were obtained?
- B. The primary cause of the failure and description of the failure mechanism
  - What is the primary cause of the failure (also provide reasoning)?
  - What's the chain of action that led to the failure?
- C. Ruling out alternate failure mechanisms
  - Can plastic deformation be ruled out? If yes, explain how.
  - Can creep be ruled out? If yes, explain how.
  - Can brittle fracture be ruled out? If yes, explain how.
  - Can fatigue be ruled out? If yes, explain how.
  - Can environmentally assisted failure be ruled out? If yes, explain how.
- D. Recommendations to prevent similar failures in the future
  - How should the design, material, use, etc. be develop to avoid similar failures in the future? Provide several alternatives and indicate most promising.

Name: Nguyen Xuan Binh  
Student ID: 887799

## Materials Safety analysis report on brittle fracture failure of axle shaft of forklift

### Problem Overview:

The report investigated the reasons for the failure of axle shafts used in forklifts. These shafts are the integral components of the rear axle, and they are pivotal in transmitting torque and maintaining wheel positions. Notably, one axle shaft, crafted from 42CrMo4 grade steel, malfunctioned after just 296 hours of service (12.3 days). The abrupt failure, marked by a sudden jerk, raised concerns about potential overloading, material integrity and manufacturing processes.

### A. Description of investigation methods applied

- **What means of investigation were used in the failure analysis?**

The author tries to determine possible if the observed inclusions are the result of brittle/ductile fracture material on the axle shaft, both in the core and on the thin case of 3-mm. From the report, the means of investigation for the failure analysis included:

1. Chemical Analysis: The chemistry of the failed axle shaft was analyzed to match with known steel grades, which is 42CrMo4 grade.
2. Micro-Hardness Testing: The micro-hardness of different locations on the failed samples was determined using a pneumatically controlled automatic micro-hardness tester.
3. Microstructural Analysis: The failed sample was etched and examined to understand its microstructure, including the presence of any inclusions or inconsistencies.

- **What computational methods were used?**

The author lists a couple of computation methods as follows:

1. Field Emission Gun Scanning Electron Microscopy (FEG-SEM): This method was used to identify the exact phases present in the samples.
2. Inclusion Rating: The failed component was rated for inclusions in ASTM E45 standards.
3. Fractography: The nature of the fracture surface was studied to determine whether it was brittle or ductile. It was shown that the core suffered from ductile fracture while the case suffered from brittle, cleavage fracture.

- **What material or results were obtained?**

**Main result:** The outer surface of the fracture showed a cleavage nature, suggesting a brittle fracture, while the inner core revealed a dimple nature, indicating a ductile fracture. Both coarse and fine pearlite structures were seen in the core due to an improper heat treatment process. Additionally, the un-etched microstructure of the shaft revealed the presence of thin and thick sulphide (Type A) inclusions with severity ratings of 2.5 and 0.5, respectively.

## B. The primary cause of the failure and description of the failure mechanism

- **What is the primary cause of the failure (also provide reasoning)?**

The primary cause of the failure is likely to be brittle fracture due to improper heat treatment. There are four main reasons for this type of failure:

- **What's the chain of action that led to the failure?**

The chronological order of the superheater tubes' failure is as follows:

1. Observations: The axle shaft failed in shear mode at almost 45° to the longitudinal direction under torque. The fracture surface had two distinct regions: a smooth annular region at the periphery where the fracture initiated and a rough core.
2. The hardening layer was found to be non-uniform across the section, and in some areas, it exceeded the specified depth (>2–3 mm).
3. The un-etched microstructure showed numerous sulphide inclusions, indicating that the steel was not clean.
4. The surface of the rod sample exhibited an inhomogeneous/banded microstructure in a martensitic matrix, while the core displayed a ferrite pearlite structure
5. The un-etched microstructure of the shaft revealed the presence of thin and thick sulphide (Type A) inclusions with severity ratings of 2.5 and 0.5
6. The difference in fracture behavior was caused by the variation in the microstructure of the case and core resulting from the improper hardening treatment.

## C. Ruling out alternate failure mechanisms

- Can plastic deformation be ruled out? If yes, explain how.

No, it cannot be ruled out due to the dimple nature of fracture in the inner core (B). Dimpled fracture surfaces are characteristic of ductile fracture and are indicative of plastic deformation prior to failure. Dimples are microscopic voids or cavities that form in the material due to the nucleation, growth, and coalescence of voids under tensile stress.

- Can creep be ruled out? If yes, explain how.

Creep can be ruled out since the report does not mention the axle shaft operating at elevated temperatures or under constant loads for extended periods. Additionally, the axle shaft failed after just 296 hours of service, which is also a short time that is uncommon for creep.

- Can brittle fracture be ruled out? If yes, explain how.

No, it cannot be ruled out since it is the main reason stated in the report.

- Can fatigue be ruled out? If yes, explain how.

Fatigue can be ruled out. The non-uniform distribution of hardness across the shaft, with a very high hardness on the surface-hardened layer, suggests that the material was more susceptible to brittle fracture. Fatigue would typically initiate at regions of stress concentration, and there's no mention of such typical fatigue initiation sites.

- Can environmentally assisted failure be ruled out? If yes, explain how.

Environmentally assisted failure can be ruled out since the report does not mention the axle shaft being exposed to any corrosive chemicals or high humidity or any harsh conditions.

#### **D. Recommendations to prevent similar failures in the future**

- How should the design, material, use, etc. be developed to avoid similar failures in the future? Provide several alternatives and indicate the most promising.

To avoid similar failures in the future, several design, material, and usage recommendations can be inferred from the paper:

1. Material selection: Choose cleaner steel grades with fewer non-metallic inclusions, especially manganese sulphide inclusions, which can act as stress concentration sites. Consider using steel grades with better resistance to brittle fracture.
2. Heat treatment process: Implement a more controlled heat treatment process to avoid the formation of both coarse and fine pearlite structures in the core, which resulted from the improper heat treatment process.
3. Quality control: Regularly inspect axle shafts in service for signs of wear, deformation, or potential failure. Non-destructive testing methods like ultrasonic testing or magnetic particle inspection can be used.

572266

## 1 Introduction

This report reviews a failure analysis that was conducted for failed axles. These axles were components of forklift in most likely a production facility as the forklifts were used to lift wire rod coils from coil yard. For more detailed analysis, one of the axle shafts were studied in the failure analysis that had fractured. No damage was reported in the other components in transmission of the forklift. According to the author of failure analysis, a sudden jerk was observed before failure that might be due to overloading. Axle shaft transmits torque from motor to wheels with sudden need for great torque when accelerating.

The failed axle shaft, with a diameter of about 7 cm, was made of 42CrMo4 steel. The axle shaft was manufactured by forging and given an induction hardening treatment to produce a 3 – 4 deep layer hardened steel. The forklift had been operated for 296 hours until failure. Further study was performed to find the root cause for failure.

## 2 Investigation methods and failure mechanisms

One of the failed axle shafts were studied in more detailed level to analyze root causes for failure. Specimen of the axle shaft's fracture end was prepared by polishing and etching. The following studies were performed:

- Macroscopic inspection.
- Microscopic inspection with optical microscope and field emission gun scanning electron microscope (FEG-SEM).
- Hardness test with pneumatically controlled hardness tester (Leco-LM247).

During macroscopic inspection, the author notes the almost 45-degree angle fracture to the axial direction of the shaft. In the photographs of the shaft, a clear zone due to induction hardening can be seen. This area should be 2 – 3 mm long, but author reports uneven and increased zone of 3 – 4 mm. In the photographs, a crack can be seen reaching from the outer edge to a crater in the shaft's core.

The microstructure and inclusions were analyzed using microscopic inspections. The author describes the etched sample form the core to have a clear ferrite pearlite structure while the shaft surface has a in-homogeneous or banded microstructure in martensitic form. Author claims that mixture of coarse and fine pearlite structure within the core of the shaft points to improper heat treatment process. Excessive hardening layer also points to improper heat treating.

The presence of inclusions was analyzed with microscopic analysis according to ASTM E45 standard. The author found type A inclusions that were most likely manganese sulfide inclusions. Elemental analysis was performed with scanning electron microscope. Type D such as oxide were also reported. The type A inclusions were in the form of strings oriented in the direction of crack propagation. This suggests poor steel quality. Inclusions act initiators for crack growth and increase probability for brittle fracture.

Finally, the hardness profile of the axle shaft was studied. The author concluded that the overall hardness profile is uneven. Average hardness was measured at 735 HV that author claims to be very high compared to the core material (in the range of 240 – 250 HV) and very high in the use

of axle shaft material. Having such high hardness makes the axle shaft brittle and vulnerable for brittle fracture mechanism.

### 3 Failure analysis

Due to all the evidence that the author has collected, the most likely primary failure mechanism is brittle fracture. Evidence points to a possible cleavage fracture due to both elements in very high material hardness and presence of inclusions.

The axle shaft was produced by forging and then heat treating with induction to create a martensite structure to the outer surface of the shaft. However, the hardness was measured as very high compared to the application as a forklift transmission axle shaft. The hardened layer was measured as uneven and larger than expected. This suggests that the axle shaft was manufactured as too brittle.

The inclusions within the 42MoCr4 point to poor quality steel. Inclusions within the steel can act as stress concentrators that initiate a crack growth. Overall fracture toughness was decreased that made the axle shaft vulnerable for brittle fracture. Core of the shaft had marks of ductile fracture, most likely due to overloading the axle shaft after the brittle fracture took place.

There are still other failure mechanisms that should be addressed and possibly ruled out as a possibility. Some of them are listed here:

- Plastic deformation can be ruled out. There is no sign that the axle was plastically deformed in any way. The core of the axle had marks of ductile fracture and deformation only on the surface of the fracture.
- Creep can be ruled out. The forklift worked most likely near room temperatures and elevated temperatures alter this mechanism. The microscopic study did not find any signs of cracks or crack propagation that would suggest creep within the material.
- Brittle fracture has been suggested as the primary failure mechanism.
- Fatigue cannot be entirely ruled out. It is very unlikely to be the only failure mechanism. The forklift had been operated for only 269 hours. According to Granta EduPack, the fatigue strength of 42CrMo4 grades does not decrease significantly as number of cycles is in the range of thousands. However, fatigue could have played a role in the chain of event and crack propagation.
- Environmentally assisted failures can be ruled out. Temperatures are assumed to be around room temperatures and no signs of corrosion were present.

For future recommendations, it is important that the quality of steel is verified. A supplier of the steel should regularly test samples and confirm that the level of inclusions is tolerable.

Manufacturing processes for the axle shaft must be reviewed, especially the induction heat treating process. The heat-treating process resulted in an uneven layer of martensite and most likely produced overall too hard top layer to the shaft axle that made the product vulnerable for brittle fracture. Overall product design should aim for softer material to avoid brittle failure. Most likely the failure is due to poor product materials and manufacturing processes which both need to be addressed.